Dissociation of deuteromethane following carbon 1*s* core ionization

E. Kukk,*
Department of Physical Sciences, University of Oulu, P.O. Box 3000, FIN-90014, Oulu, Finland

J. Rius i Riu
SCFAB, Section of Atomic and Molecular Physics (KTH), Roslagstullsbacken 21, 106 91, Stockholm, Sweden

M. Stankiewicz
Instytut Fizyki im. Mariana Smoluchowskiego, Uniwersytet Jagielloński, ul. Reymonta 4, 30-059 Kraków, Poland

P. A. Hatherly
J.J. Thomson Physical Lab, University of Reading, Whiteknights, P.O. Box 220, Reading, RG6 6AF, United Kingdom

P. Erman, and E. Rachlew
SCFAB, Section of Atomic and Molecular Physics (KTH), Roslagstullsbacken 21, 106 91, Stockholm, Sweden

P. Winiarczyk
Instytut Fizyki im. Mariana Smoluchowskiego, Uniwersytet Jagielloński, ul. Reymonta 4, 30-059 Kraków, Poland

M. Huttula and S. Aksela
Department of Physical Sciences, University of Oulu, P.O. Box 3000, FIN-90014, Oulu, Finland
(Received 8 March 2002; published 15 July 2002)

Energy-resolved electron-ion coincidence spectra of the deuteromethane molecule were measured following ionization by narrow-band synchrotron radiation. The ion mass spectra were recorded in coincidence with the outer and inner valence photoelectrons and with the normal Auger electrons from the decay of the carbon 1*s* core hole. Complementary noncoincidence ion mass spectra were measured below and above the C 1*s* threshold. The fragmentation patterns of the singly and doubly ionized deuteromethane under different ionization conditions are examined. Carbon core ionization is shown to open new photodissociation pathways not available in the valence ionization photon energy regime. With the aid of *ab initio* quantum chemistry calculations, a two-step model of the dissociation following core ionization is proposed, showing a good agreement with the experimental findings.

DOI: 10.1103/PhysRevA.66.012704 PACS number(s): 33.80.Eh, 82.80.Rt, 33.80.Gj

I. INTRODUCTION

Photoionization and absorption processes often damage the molecular bond structure to such an extent as to result in a complete or partial fragmentation of the molecule. The availability of tunable synchrotron radiation makes it possible to selectively remove electrons from different molecular valence orbitals or deeper atomiclike core levels. The photon energy dependence of the dissociation processes can be studied by detecting the produced fragments using the ion time-of-flight (TOF) technique, for example. However, one is ultimately interested in tracing back every detected dissociation event to a particular type of the photoionization or excitation event. In order to achieve this goal, coincidence measurements are needed [1]. In particular, detecting photoelectrons or Auger electrons in coincidence with the ionic fragments of the molecule provides us with a detailed and highly differential picture of the molecular dynamics following the absorption of monochromatic synchrotron radiation. Such studies in gas-phase put high requirements on the experimental apparatus and light sources due to the inherently low count rates of the coincidence measurements.

Extensive knowledge has been gathered about the molecular dissociation following UV ionization of the outer molecular orbitals (see Ref. [2] and references therein). A number of experimental as well as theoretical studies exist on the dissociation of the methane molecule under various valence-level excitation conditions [3–8]. Less is known about the processes taking place after the creation of a core hole (Ref. [9] and references therein). A considerably greater amount of energy is deposited in the molecule by core-level photoabsorption than by valence absorption. As a result, fast electronic relaxation processes (mostly Auger transitions in lighter elements) follow, creating multiply ionized molecules in well-defined electronic states and providing unique starting conditions for the molecular dissociation. New dissociation pathways and many-body reactions become possible [10,11]. Core ionization is also followed by nuclear relaxation towards the equilibrium of the core-hole state, which competes in time with the electronic relaxation [12] and can have an effect on the eventual breakdown of the molecule. Studying the nuclear dynamics after core-hole creation can reveal new aspects not accessible in the UV excitation re-

*Electronic address: Edwin.Kukk@oulu.fi

gime, as observed for example in the CF_4 [13], CO_2 [14,15], and H_2O [16] molecules.

Here, we present experimental results on the molecular fragmentation following carbon 1*s* core ionization in the deuterated methane molecule. The isotopic substitution of the hydrogen was used to enhance the ion mass resolution of the experiment. The ionic fragments were detected in coincidence with the Auger electrons, eliminating the electronic processes other than the core ionization and subsequent Auger decay to the selected doubly ionized states. The results are compared with the fragmentation patterns recorded below the C 1*s* threshold following selective ionization of the outer molecular orbitals. As complementary results, noncoincidence measurements of the ionic fragments below and above the C 1*s* threshold are also presented. The results are interpreted on the basis of quantum chemical calculations of the molecular structure and dynamics, focusing on the doubly ionized molecule created by the electronic Auger decay.

II. EXPERIMENT

The measurements were carried out at the I411 undulator beamline of MAX-II laboratory (Lund, Sweden). The beamline is equipped with a modified SX-700 plane grating monochromator and efficient differential pumping stages between the end station and beamline, for gas-phase measurements [17].

The experimental setup for the energy-resolved electron-ion coincidence (EREICO) measurements is described in detail elsewhere [18]. It comprises of a 125-mm electrostatic hemispherical electron energy analyzer Omicron EA125 (EA) coupled with a 120-mm free drift length, modified Wiley-McLaren type of ion TOF analyzer. The EA is equipped with five channeltron detectors, placed along the dispersive direction. A confined gas source, which is an integral part of the TOF spectrometer, provides target gas pressures 10–100 times above the chamber pressure. During the measurements the chamber pressure is kept below 6×10^{-6} mbar. Different pass energy and entrance slit combinations of the EA allow us to select suitable electron kinetic-energy resolution. In order to perform the EREICO measurements, first the electron energy spectrum of the region of interest is measured at the selected photon energy with a pass energy and entrance slit combination providing sufficient energy resolution. The kinetic energy of the electron peak with which the ion coincidence spectra will be measured is then determined. The voltages of the EA are set manually to correspond to the selected kinetic energy and are kept constant during the following coincidence measurement. For these, the commercial data-acquisition system of the EA is replaced so that the electrons detected by the channeltrons of the EA provide the start signal for the time-of-flight measurements and the ions detected by the TOF analyzer are used as the stop pulses for the time-to-digital converter card (model 7886 by FAST Comtec). The card is installed in a personal computer (PC) with the appropriate software for data acquisition, storage, and display. For the present EREICO measurements, three channeltrons out of the array of five were used for obtaining a common start signal.

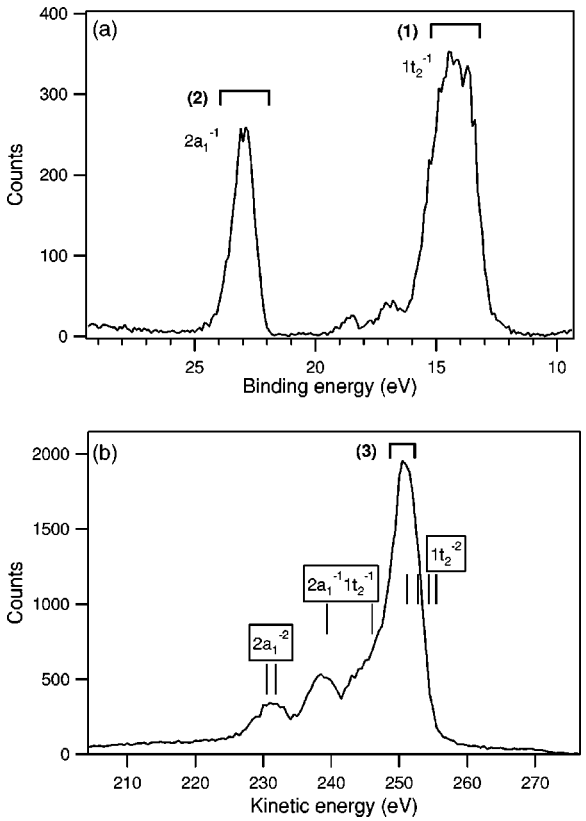

FIG. 1. (a) Valence photoelectron spectrum of CD_4, measured at $h\nu = 70$ eV. (b) Normal Auger-electron spectrum measured at $h\nu = 350$ eV. Vertical bars mark calculated energies of the CD_4^{2+} final electronic states and horizontal brackets (1)–(3) indicate the electron energy windows for the EREICO measurements.

A complementary set of noncoincidence ion yield measurements was performed at the undulator beamline U49/1-SGM of BESSY-II, Germany, using an ion time-of-flight spectrometer developed at the University of Oulu [19]. This Wiley-McLaren-type spectrometer uses a pulsed field (20 kHz) ion extraction from the interaction region. The extraction pulses serve as the start signal for the time-digital converter PC card that then stores the ion flight times from the multiple stop pulses from the multichannel plate detector. The spectrometer has been optimized for good mass resolution and therefore the peak broadening due to the kinetic energy of the ions is negligible. The mass resolution of the spectrometer was found to be about 1% for the present measurement. Due to the strong electric field (≈ 1 kV/cm) in the source volume, the transmission of the spectrometer is very high and virtually all ions are collected.

III. EXPERIMENTAL RESULTS

A. Energy-resolved electron-ion coincidence (EREICO) measurements

Electron energy spectra measured prior to the EREICO measurements are presented in Fig. 1. The valence photo-

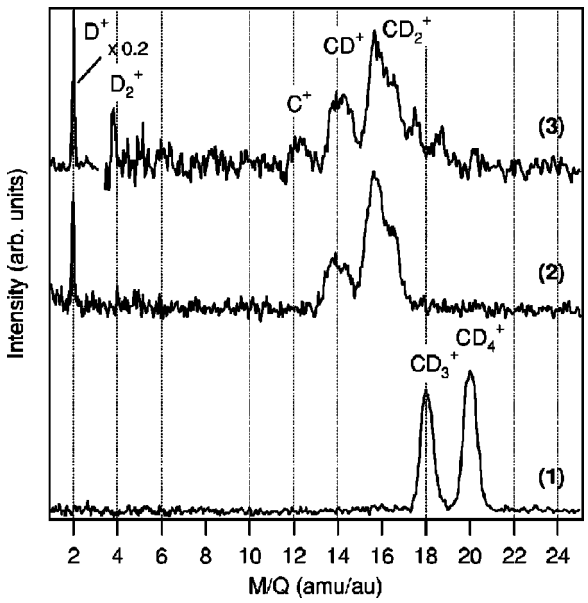

FIG. 2. Energy-resolved electron-ion coincidence (EREICO) spectra of CD_4. The ion mass spectra (1) and (2) are measured at $h\nu=70$ eV in coincidence with the $1t_2$ and $2a_1$ photoelectrons, correspondingly. Spectrum (3) is measured in coincidence with Auger electrons at $h\nu=350$ eV.

electron spectrum, measured at $h\nu=70$ eV, is shown in Fig. 1(a); the normal Auger spectrum, measured at $h\nu=350$ eV, is shown in Fig. 1(b). The spectra were recorded using the 40-eV and 70-eV pass energy of the EA for the photoelectron and Auger electron spectra, correspondingly. The electron energy resolution of these spectra [1.0 eV in Fig. 1(a) and 1.9 eV in Fig. 1(b)] equals that of a single channeltron detector.

The neutral ground state of CD_4 has the electron configuration of $1a_1^2 2a_1^2 1t_2^6$ in the tetrahedral T_d symmetry [20,21], where the $1a_1$ molecular orbital resembles closely the atomic carbon $1s$ orbital and will be hereafter referred to as such. The spectrum in Fig. 1(a) shows the outer valence photoelectron line $1t_2$ with mostly unresolved Jahn-Teller-split components and the inner valence line $2a_1$ [22–24]. The normal Auger final states of the spectrum in Fig. 1(b) belong to the $1a_1^2(2a_1 1t_2)^6$ configurations. The assignment of this spectrum was done already by Ortenburger and Sagus [25]. The individual energy levels that are shown in the figure are from our *ab initio* calculations, described in Sec. IV. The dominant structure corresponds to the $1a_1^2 2a_1^2 1t_2^4$ configuration, which has four energy levels. The horizontal brackets in Fig. 1 mark the positions and approximate widths of the energy windows from where the electrons were detected in coincidence with the ions in the following EREICO measurements.

The EREICO spectra are presented in Fig. 2 after converting the original time-of-flight scale into the ion mass/charge scale using the relation $T\propto\sqrt{M/Q}$. The ions in spectra (1)–(3) were measured in coincidence with the electrons from the regions (1)–(3) of Fig. 1. The resolution of the EA in the EREICO measurements was lower than for the noncoincidence electron energy spectra taken under identical settings, since a common electron signal was obtained from three detectors. Taking into account the spacings of the channeltrons along the dispersive direction of the detection plane and the analyzer's dispersion, the estimated resolution for the 40-eV pass energy [spectra (1)–(2)] is about 2.0 eV and for the 70 eV [spectrum (3)] about 3.5 eV. Spectra (1) and (2) correspond to ion production following the ionization of the $1t_2$ and $2a_1$ molecular orbitals, respectively, with 70-eV photons. Spectrum (3) shows ions produced after the normal Auger transitions to a doubly ionized final state $1t_2^{-2}$. The three spectra exhibit very different dissociation patterns, summarized in Table I. The valence photoionization of the $1t_2$ orbital results mostly in a stable molecular ion CD_4^+, corresponding to the observed peak at 20 amu. However, nearly half of the CD_4^+ ions dissociate into CD_3^+ and neutral D fragments (not detected). There is no observable dissociation into lighter fragments CD_n^+ $(n=0-2)$, nor is there evidence of the $CD_4^+\rightarrow CD_3+D^+$ process. Ionization of the inner valence orbital $2a_1$ [spectrum (2)] results in a more complete fragmentation of the molecule—there are no stable parent CD_4^+ ions or CD_3^+ fragments. Mostly the CD_2^+ and in a lesser extent the CD^+ fragments are produced. A notable difference from spectrum (1) is also the presence of the D^+ ions that can originate from the $CD_n^+\rightarrow CD_{n-1}+D^+$ type dissociation. Quite different fragmentation processes follow the Auger decay [spectrum (3)], in which two holes are cre-

TABLE I. Relative abundances of ions from the TOF spectra of CD_4. The electronic state corresponding to the coincidence electrons is given for the EREICO measurements.

$h\nu$ (eV)	Electronic configuration	C^+	CD^+	CD_2^+	CD_3^+	CD_4^+
EREICO measurements						
70	$1t_2^{-1}$				0.45	0.55
70	$2a_1^{-1}$		0.25	0.75		
350	$1t_2^{-2}$	0.06	0.25	0.51	0.18	
Ion yield measurements						
350		0.21	0.27	0.38	0.12	0.02
260		0.04	0.22	0.35	0.20	0.20
difference [a]		0.23	0.28	0.39	0.11	0.00

[a]From the spectrum at $h\nu=350$ eV after subtracting the spectrum at $h\nu=260$ eV, normalized to the equal intensity of the CD_4^+ peak.

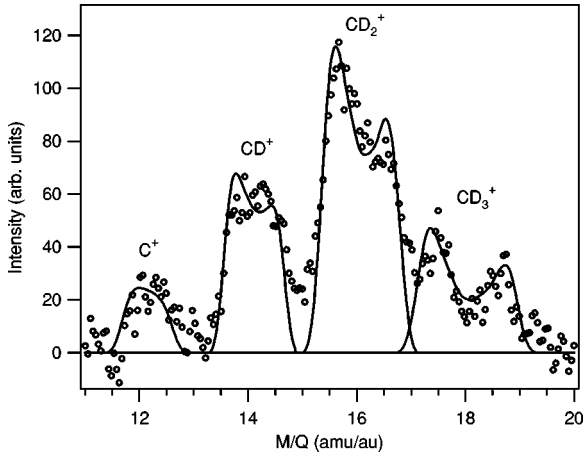

FIG. 3. A region of the EREICO spectrum (3) of Fig. 2 (circles, $h\nu = 350$ eV, ions in coincidence with Auger electrons) together with simulated peak shapes (lines).

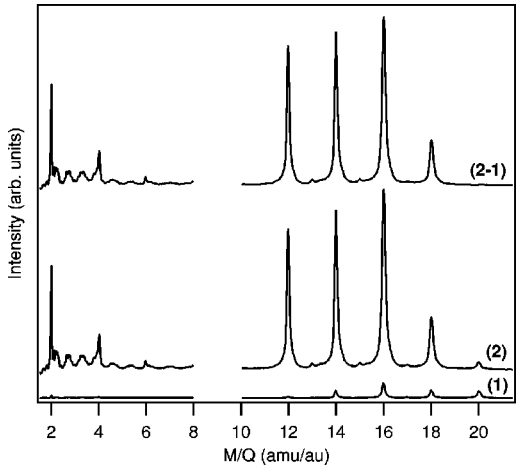

FIG. 4. Ion mass spectra of CD_4 measured at the photon energy of 260 eV (1) and 360 eV (2), normalized to the equal intensity of the CD_4^+ peak. The difference spectrum (2-1) is given on top.

ated in the valence $1t_2$ orbital. The major fragment ion here is CD_2^+, with CD^+ and C^+ also present, and some structure corresponding to CD_3^+. Here, too, the D^+ ions are observed, but in addition a weak signal appears at 4 amu, corresponding to the D_2^+ ions.

The peak shapes in the EREICO spectra of Fig. 2 are strongly influenced by the kinetic energy of the ions. The voltage applied across the interaction region for directing the ions into the TOF analyzer is relatively low [4 V for spectra (1) and (2) and 16 V for spectrum (3)] and there is a delay in entering the analyzer for the ions moving initially away from it. This results in peak broadening and even splitting in the case of fast ions. Under the present experimental settings, the kinetic-energy release in the dissociation is the most important factor for determining the TOF peak shape. In order to determine the kinetic energy of the ions, Monte Carlo peak shape simulations were performed. These simulations take into account the ion time of flight from its creation to its detection, including the delay introduced by our data-acquisition electronics and the electron time of flight from its emission to its detection in the electron analyzer. The ions for the Monte Carlo simulation are generated according to a given kinetic-energy distribution and are emitted isotropically. This energy distribution is then adjusted until the best fit to the measured ion TOF peak is obtained. The simulations also account for the finite size of the source volume and the photon beam, but since space focusing conditions are fulfilled, these factors have only a minor effect on the peak shape.

In spectrum (1), the peaks are relatively narrow, inferring ion kinetic energies less than 0.02 eV. The peak shapes are quite different in spectrum (2); they consist of two components, corresponding roughly to the ions moving towards and away from the TOF analyzer. Fitting with simulated shapes gave the kinetic energies of about 0.2 eV for both the CD^+ and CD_2^+ peaks. The region of the heavier fragments of the spectrum (3) is shown in Fig. 3 together with simulated peak shapes. As for spectrum (2), strong broadening due to high kinetic energy of the ions is seen and in the case of the CD_3^+ ion, the peak is clearly split into two components. The kinetic energies obtained from the simulation are the following: 0.5 eV (C^+ and CD^+), 0.7 eV (CD_2^+), and 0.9 eV (CD_3^+). Note that the voltages applied across the interaction region are higher for spectrum (3) than for (1) and (2) and thus similar peak widths in spectrum (3) correspond to considerably larger kinetic energies. In order to better represent the experimental spectrum, the ions were assigned a certain Gaussian kinetic-energy spread centered at the above-given values. This spread can be viewed as due to the projection of the Auger initial state's nuclear wave function onto the potential-energy surfaces of the doubly ionized Auger final states and was found to be about 0.5–0.6 eV (full width at half maximum). The light ion of D^+ has an exceptionally narrow peak in spectra (2) and (3), although it probably has high kinetic energy as well. A large fraction of these ions escapes detection and the voltages in the interaction region are sufficient only to collect the ones with the initial velocity within a narrow cone towards the analyzer.

B. Ion yield measurements

The EREICO measurements allow one to select precisely the electronic state from which to study the dissociation process. As a drawback, the coincidence count rates are quite low and the spectra have poor statistics. We performed additional noncoincidence ion yield measurements, using a Wiley-McLaren-type ion TOF spectrometer. The spectra, converted to the M/Q scale, are shown in Fig. 4 for the ionizing photon energy below [spectrum (1)] and above [spectrum (2)] the C $1s$ threshold. These spectra represent ions from all photoionization and excitation processes possible at the given photon energy. Spectrum (1) is mostly a result of the $2a_1$ and $1t_2$ direct ionization, possibly with contributions from double ionization and satellite excitations. Spectrum (2) follows mostly the C $1s$ ionization and Auger decay, with a much weaker contribution from direct $2a_1$ and $1t_2$ ionization. In addition to the peaks associated with CD_4, the spectra exhibit some spurious oscillations in the region between 2 and 6 amu due to electronic noise.

In order to compare these noncoincidence results with the ion–Auger-electron EREICO measurements, the contribution from valence ionization was subtracted from the spectrum (2) of Fig. 4 as follows: It is not possible to produce the CD_4^+ fragment following the Auger decay, which creates the CD_4^{2+} ions. The CD_4^+ peak in spectrum (2) is therefore entirely due to valence ionization. The relative intensities of the other peaks from valence ionization can be assumed to be the same at $h\nu = 260$ eV and 350 eV. Subtracting spectrum (1) from spectrum (2) after normalizing them to the equal intensity of the CD_4^+ peak leaves a spectrum [marked (2-1) in Fig. 4], representing only the dissociation following core ionization (see also Table I). Comparing this spectrum with the EREICO spectrum (3) of Fig. 2 shows that there is a larger fraction of lighter fragments present in the noncoincidence spectrum, particularly the C^+ production is much higher. This seeming discrepancy can be explained by taking into account that all possible Auger final states $1a_1^2(2a_1 1t_2)^6$ contribute to the noncoincidence TOF spectrum, whereas the EREICO spectra relate mainly to the $1a_1^2 2a_1^2 1t_2^4$ states. The dissociation pathways producing lighter fragments could be preferred after the Auger decay to the higher-energy $1a_1^1 2a_1^1 1t_2^5$ and $1a_1^2 2a_1^0 1t_2^6$ states. This is a reasonable assumption considering that also the direct photoionization of the $2a_1$ orbital results in a more complete fragmentation than the ionization of the $1t_2$ orbital, supported by the very recent results by Fainelli *et al.* [11]. A similar shift towards stronger fragmentation has been observed in the case of NH_3, when populating higher-lying doubly ionized states [9] and is considered to be a general tendency [11]. Another notable difference is that the D_2^+ peak appears to be more intense in the noncoincidence measurements above the C $1s$ threshold [spectrum (2), Fig. 4] than in the EREICO spectra [spectrum (3), Fig. 2]. Also a weak signal corresponding to the D_3^+ ions appears. This suggests that if higher-energy Auger final states of the $1a_1^1 2a_1^1 1t_2^5$ and $1a_1^2 2a_1^0 1t_2^6$ configurations are reached, new dissociation processes, such as $CD_4^{2+} \rightarrow CD_2^+ + D_2^+$ and $CD_4^{2+} \rightarrow CD^+ + D_3^+$, gain importance.

IV. CALCULATIONS AND DISCUSSION

A. Initial assumptions

The aim of the present calculations was to find the most likely path of dissociation the molecule follows after core ionization. It is important to clarify the initial conditions for the dissociation, as on the femtosecond timescale there is an interplay between electronic and nuclear relaxations after the core ionization. On one extreme, the core-hole decay can be so rapid that no changes in the molecular geometry occur before the double valence hole Auger final electronic state is created. In such a case, the molecular dissociation would start from the well-known neutral ground-state geometry. If, at the other extreme, the core-hole state has time to find its equilibrium before the Auger decay takes place, the dissociation would start from a different core-hole state geometry. These simultaneous processes would be properly represented by a one-step coupled model of the core ionization or core excitation, Auger decay, and nuclear motion [12,26]. However, assuming fast nuclear relaxation of the core-hole state prior to the Auger decay seems to give satisfactory computational results in cases like CO under typical experimental conditions [27]. In this work, we also assume the relaxed geometry of the core-hole state as the starting point for the dissociation. As a further approximation, the vibrational motion in the core-ionized state is not taken into account, i.e., the molecule is assumed to be ''frozen'' initially.

The molecule can start to dissociate already in the core-hole state, as observed for HCl, for example (see Ref. [28] and references therein). In the case of CD_4, however, this is unlikely, since the core-hole state is bound according to calculations [29], which are confirmed by the observed vibrational progression in the C $1s$ photoelectron spectrum of methane [30]. In brief, we assume the following sequence of events: (1) Core-ionization of the neutral deuteromethane. (2) Nuclear relaxation of the core-hole ionic state to its equilibrium geometry. (3) Auger decay, creating two holes in the valence $1t_2$ orbital. (4) Nuclear relaxation of the doubly ionized state, eventually leading to the fragmentation of the molecule.

B. The molecule and its fragments

Let us first consider the deuteromethane molecule in various relevant electronic states prior to the dissociation and its fragments after the dissociation is complete. The ground state of CH_4 (CD_4) is well known to have tetrahedral symmetry with the C-H bond length of 1.0873 Å [31]. In Table II are given the properties of the neutral ground state of CD_4 and of the singly and doubly ionized molecule as well as of some of its dissociation products. In the following, we use the energies and geometries obtained using multiconfiguration self-consistent-field (MCSCF) approach in the complete-active-space optimization employing the cc-pVDZ basis set [32](except for the core-ionized molecule) for the sake of regularity, even if in some cases more accurate experimental or theoretical values are available. The calculations were performed using the DALTON quantum chemistry code [33].

The C $1s$ core ionization does not destroy the ground-state symmetry, but results in shortening of the C-D bonds from 1.087 Å to 1.032 Å [31,34] in the $1a_1^1 2a_1^2 1t_2^4 (^2A_1)$ state. In contrast, valence ionization of the $1t_2$ orbital creates an electronic state that is subject to Jahn-Teller distortions [35]. As the Jahn-Teller theorem states, ''for a nonlinear molecule in an electronically degenerate state, distortion must occur to lower the symmetry, remove the degeneracy, and lower the energy'' [36]. We obtained a nuclear equilibrium geometry for the lowest doublet state (without preserving any of the symmetry elements), which is very close to the C_{2v} symmetry, with the C-D_n bond lengths of 1.21 Å ($n=1,2$), 1.08 Å ($n=3$), and 1.10 Å ($n=4$). The small deviation from the C_{2v} symmetry can probably be attributed to the deficiencies of the rather small basis set. Our result is in good agreement with recent calculations by Takeshita [37], where similar parameters in the C_{2v} geometry were obtained for the lowest CH_4^+ state $^2B_1$.

TABLE II. Properties of the CD_4 molecule in its neutral and ionized states and of its fragments. The energies and equilibrium bond lengths are from MCSCF calculations, unless noted otherwise. Lowest-energy singlet or doublet states are given.

Molecule/ fragment	Energy (H)			R_e(Å)	Note
	Electronic	Vibrational	Total		
CD_4	−40.281	0.032	−40.249	1.11	T_d geometry
CD_4		0.032		1.09	[31,43] mass corrected
$C^*D_4^+$		0.035		1.04	core ionized [29,34]
CD_4^+	−39.819	0.028	−39.791	1.21; 1.09	
	−39.873			1.19; 1.09	[37]
CD_4^+			−39.748	1.09	ground-state geometry
CD_4^{2+}	−39.148	0.026	−39.122	1.32; 1.15	equilibrium, planar
			−38.823	1.04	core-ionized geometry
			−38.875	1.09	ground-state geometry
CD_3^+	−39.280	0.023	−39.256	1.11; 1.09	
				1.09	[40]
CD_2^+	−38.664	0.012	−38.652	1.11	
				1.11	[41]
CD^+	−37.998	0.005	−37.992	1.14	
C^+	−37.357		−37.357		
D_3	−1.636	0.008	−1.632	0.95	
D_3^+	−1.343				[44]
D_2	−1.163	0.007	−1.156	0.76	
	−1.174	0.007	−1.167	0.74	[43,45]
D_2^+	−0.600	0.004	−0.596	1.05	
D	−0.500		−0.500		

The Auger decay of the core hole creates the electron configurations of $1a_1^2(2a_1 1t_2)^6$ in the T_d geometry. As seen from the normal Auger spectrum (Fig. 1) and according to calculations [25,38], mostly the $1a_1^2 2a_1^2 1t_2^4$ configuration is populated. There are four terms in the $1t_2^{-2}$ configuration, $T_2 \otimes T_2 = ({}^3T_1, {}^1E, {}^1T_1, {}^1A_1)$, from which mostly the singlet states ^1E and $^1T_1$ are populated by the Auger transition, the $^1A_1$ state having much less intensity [38]. As electrons are removed from the degenerate $1t_2$ orbital, the molecule undergoes Jahn-Teller distortions destroying the T_d symmetry. There are several possible new equilibria in the lower symmetry. In Table II, the optimized geometry of the lowest singlet state of the CD_4^{2+} ion is given, obtained from energy minimization of the lowest singlet ^1E state in the C_{2v} symmetry. The same nuclear configuration was arrived at also in an optimization without preserving any symmetry elements. The new equilibrium corresponds to a planar molecule, with the C-D_n bond lengths of 1.32 Å ($n=1,2$) and 1.15 Å ($n=3,4$) and the angles of 42.6° (D_1-C-D_2), 126.2° (D_3-C-D_4), and 95.1° (D_2-C-D_3, D_1-C-D_4). This energy minimum can indeed contain bound states, as verified by vibrational analysis. A planar geometry was also predicted for AH_4 systems with six valence electrons, such as CD_4^{2+} by Saturno [39], both in its lowest-energy (triplet) state and first excited state. With the vertical transitions from the ground and core-ionized state in mind, we also calculated the energy of CD_4^{2+} for the lowest singlet state ^1E at the corresponding tetrahedral configurations (Table II).

A number of molecular fragments can be produced by the dissociation. Their geometry-optimized energies are also listed in Table II. The lowest singlet state of CD_3^+ was found to have a planar geometry with the D-C-D angles of 120° and the C-D bond lengths of 1.11, 1.11, and 1.09 Å. With a larger basis set, one would again probably arrive at equal bond lengths and the exact D_{3h} symmetry. The present result is in good agreement with Ref. [40], where a planar configuration with 1.087-Å C-H bond length was found for CH_3^+.

The next fragment, CD_2^+, has a 1.11-Å bond length and a 139° bond angle, in a good agreement with Ref. [41]. The last heavy molecular fragment, CD^+, has a 1.14-Å optimized bond length. The neutral fragments CD_n ($n=0-3$) are not listed in Table II, since their production is unlikely and they cannot be observed in our experiment.

C. Molecular dissociation

1. Primary dissociation

The vertical Auger transition from the core-ionized equilibrium onto the potential-energy surface of the doubly ionized state leaves the ion with the excess energy of more than 8 eV above its zero-point energy (Table II). In order to follow the dissipation of this energy, a so-called dynamic walk was performed. In this procedure [42], the force vectors on each atom are calculated at the given initial nuclear geometry after optimizing the electronic structure. Then, small displacements of the nuclei are performed according to the

TABLE III. Primary and secondary dissociation reactions following C 1*s* core ionization and Auger decay and their energy release ($E>0$) or required dissociation energy ($E<0$).

Number	Reaction	Energy (eV)
1	$CD_4^{2+} \rightarrow CD_3^+ + D^+$	11.8
2	$CD_4^{2+} \rightarrow CD_2^+ + D^+ + D$	9.0
3	$CD_4^{2+} \rightarrow CD_2^+ + D_2^+$	11.6
4	$CD_3^+ \rightarrow CD_2^+ + D$	−2.8
5	$CD_3^+ \rightarrow CD^+ + D_2$	−2.9
6	$CD_3^+ \rightarrow C^+ + D_2 + D$	−6.6
7	$CD_2^+ \rightarrow CD^+ + D$	−4.4
8	$CD_2^+ \rightarrow C^+ + D_2$	−3.8
9	$CD^+ \rightarrow C^+ + D$	−3.6

force field. The process is repeated interactively—the electronic structure is reoptimized, the nuclei shifted—until the molecule dissociates. The procedure is semiclassical in the sense that it does not quantize the vibrational motion of the molecule, which behaves as a classical oscillator.

The molecular dynamics was simulated by the dynamic walk following several different initial conditions and using different basis sets, although for the final results, the cc-pVDZ basis was used. The starting geometry was either that of the neutral ground or of the core-ionized state. In both cases the vibrational motion of the molecule at the beginning of the walk was not taken into account—the nuclei had no initial momenta. If at least one symmetry element was preserved (the C_s group) during the dissociation, then a three-particle fragmentation to CD_2^+, D^+, and D takes place (process 2 in Table III). However, if no symmetry restrictions were imposed on the molecule, then a different process (1) (Table III) occurs, producing singly charged CD_3^+ and D^+ fragments. Whereas the dissociation path (2) corresponds to the strongest ion peak observed in the EREICO spectra (Fig. 2), it does not explain the presence of the CD_3^+ fragments. Also, the preservation of a reflection plane has no obvious justification, and thus we base the following discussion on the results obtained without symmetry restrictions.

Following the nuclear dynamics of CD_4^{2+}, it was apparent that several vibrational modes became strongly excited as the ion relaxes towards its equilibrium geometry. At first, the nonquantized vibrational motion of the dynamic walk can be regarded as a Jahn-Teller distortion, lowering the T_d symmetry towards a planar configuration. So much energy is released in this initial stage, however, that the molecule dissociates. The details of the nuclear motion depended on the type of calculation—the used basis set, size of the active space, etc. However, in all performed calculations the end result was the same—a D^+ fragment was ejected from the ion at the moment when the vibrational modes combine with suitable phases (in the order of 100 fs after Auger decay). No principal differences were found when following the dynamics of the two lowest-energy electronic terms of CD_4^{2+}. This suggests that the dissociation dynamics and mechanisms are similar for the lower-energy terms of CD_4^{2+}, although we consider here only the lowest-energy singlet term of CD_4^{2+}.

Starting at the ground or core-ionized geometry does not change the final result. This is to be expected, as the available kinetic energies do not differ much (about 12 eV from the core-ionized geometry and 10 eV from ground-state geometry). After the dissociation barrier is crossed, the Coulomb repulsion between the fragments gives them quite high translational energy (about 6 eV in our calculations). The rest (also about 6 eV) is confined in the CD_3^+ fragment mainly as vibrational excitations. The energies in Table III should be taken as guidelines for qualitative arguments rather than as accurate values. Particularly the division of the released energy between the translational and vibrational kinetic energies probably varies considerably, since it is dependent on the particular moment of the vibrational motion of the parent ion, when the ejection of the D^+ fragment occurs. This in turn depends on in which state of the vibrational motion the *core-ionized* molecule was at the moment of the Auger transition. It has been shown, for example, that in the case of CF_4 the vibrations of the core-excited state can affect the outcome of the dissociation process [13]. Moreover, it can be seen from the vibrational progression of the C 1*s* photoelectron spectrum [30] that there is a high probability to excite the higher levels of the symmetric stretch v_1 vibrations of the core-hole state. These vibrations were not taken into account in our dynamic walk procedure, where the nuclei are at rest at the initial configuration. The ratio of the translational and vibrational energy might also depend on which term of the initial $1t_2^{-2}$ configuration to follow, as their Jahn-Teller distorted equilibrium geometries are different and thus also the excitations of the vibrational modes.

According to the dynamic walk, one expects the process $CD_4^{2+} \rightarrow CD_3^+ + D^+$ to take place as the primary dissociation event, creating fragments with high kinetic energy. This is indeed supported by the coincidence measurements, where the weak CD_3^+ peak is split due to the high kinetic energy of the fragment. It is energetically possible to have dissociation of CD_4^{2+} producing also the D_2^+ or D_3^+ fragments. These processes, although of large energy release, are not likely according to our calculations, supported also by the very small intensity of the D_2^+ or D_3^+ peaks in the experimental EREICO spectra.

2. Secondary dissociation

The CD_3^+ ion is stable in its ground state and needs about 3 eV of energy for dissociation (Table III). However, after the primary dissociation event (1), the CD_3^+ ion is left in a highly vibrationally excited state. It is very likely that the excess vibrational energy (6 eV from the simulation) is sufficient to complete the fragmentation processes (4) and (5) (Table III) and to produce the CD_2^+ and CD^+ fragments in a secondary dissociation event. The process (6) yielding C^+ seems to require slightly more energy than is available, but as the vibrational energy of CD_3^+ is expected to vary considerably and allowing for the inaccuracy of the calculations, it should be included as a possible dissociation channel. The secondary dissociation of CD_3^+ yielding neutral CD_n (*n*

$=0-2$) fragments requires considerably more energy than the processes listed in Table III [4] and is less likely to take place.

The translational energy release in the secondary processes (4)–(6) is smaller than in the primary event. In a simple picture, smaller translational energy release is partly due to the lack of Coulomb repulsion in the secondary dissociation. However, one should keep in mind that the CD_3^+ ion already has high kinetic energy from the primary event, preserved by the center of mass of its secondary dissociation products. The observed broadness of the peak shapes for the CD_n^+ ($n=0-2$) ions reflects that high kinetic energy. Furthermore, according to the experiment, the kinetic energy of the fragments CD_n^+ decreases towards smaller n. This can also be explained by the two-step picture of the dissociation. As discussed above, the energy converted into translational motion of the fragments can probably vary in a broad range up to the maximum of about 12 eV. The more of the energy is released as translational in the primary dissociation (1), the less vibrational energy is available for the second-step dissociation. Thus, the faster the CD_3^+ fragment, the less likely it is to dissociate into the lighter CD_n^+ ions. In other words, producing lighter fragments consumes more energy for breaking the C-D bonds. Therefore the observed heavier fragments tend to have higher kinetic energies than the lighter ones. The kinetic energy of the CD_3^+ fragment was found to be 0.9 eV and thus the total kinetic energy released in reaction (1) is 9 eV and, since the calculated total energy release in this reaction is 11.8 eV (Table III), the vibrational excitations of the CD_3^+ fragment amount for less than 3 eV. This is, according to Table III, insufficient to dissociate the fragment further [except by reaction (4) with 2.8-eV dissociation energy, but allowing for the experimental and calculational error bars, the available energy can well remain below the threshold also for this reaction]. If, on the other hand, the primary dissociation (1) follows a route in which <9 eV of translational kinetic energy is released, further dissociation of the created slower CD_3^+ fragments takes place. Thus, the proposed dissociation scenario and the calculated energies agree well with the experimentally determined kinetic energy of the CD_3^+ fragment.

The second step, in which the translational energy release is smaller, does not contribute significantly to the kinetic energy of the final CD_n^+ fragment, assuming that there is no directional correlation between the primary and secondary events. If the lighter fragments would be created directly in the primary dissociation event, the decrease of kinetic energy for the lighter fragments would not be obvious. A number of possible processes could contribute to the production of CD_2^+, CD^+, and C^+. For example, the energy release in the process (3) yielding CD_2^+ would be equal to that of process (1) for CD_3^+. While it is apparent that the primary fragment CD_3^+ has a very high probability to dissociate further, predicting the relative abundances of the final fragments is more difficult. One expects a secondary process to be more likely to occur if the required energy is smaller. Thus, according to Table III, the probabilities to produce CD_2^+ and CD^+ ions are about equal, while the C^+ production is less likely. The CD^+ and C^+ fragments can appear also as further dissociation [processes (7)–(9)] of CD_2^+, following the process (4). This sequence of processes requires more available energy, because no bound D_2 fragments remain, and its contribution to the dissociation is probably minor.

Our two-step model of dissociation can be compared with earlier results from photoion-photoion coincidence measurements [10], where the dissociation of the ^1E state of CH_4^{2+} was best described by the reaction $CD_4^{2+} \rightarrow CD_2^+ + H^+ + H$ (as a single dissociation pathway). The authors found a so-called Coulomb repulsion model most suitable, giving large kinetic energy to the ionic fragments and very little to the neutral hydrogen. Our approach agrees well with these observations, although the hydrogenic fragments would be ejected sequentially, not simultaneously, and alternative dissociation channels are possible. The time delay before ejecting the second, neutral hydrogen fragment would not be visible in the ion time-of-flight spectra as long as the secondary event takes place before the CD_3^+ ion enters the acceleration stage of the TOF analyzer. The time scale of the dissociation is probably in the same range as the frequency of vibrational oscillations—in the order of 100 fs or less, which is much shorter than the time needed to collect ions from the interaction region into the TOF analyzer.

3. Dissociation following valence ionization

For comparison, let us briefly consider the dissociation of a molecule with a single hole in the valence $1t_2$ orbital. Following vertical transition from the neutral ground state, the nuclear geometry of the ion starts to relax towards one of the three Jahn-Teller-split components; their relative contribution to the photoionization cross section is determined by the Franck-Condon factors between the ground state and the corresponding geometries. According to calculations, there are two stable Jahn-Teller components, which are seen as vibrational progression in the photoelectron spectrum (contained in the single $1t_2$ peak of the low-resolution spectrum in Fig. 1) [37]. A principal difference between direct ionization and Auger decay is that in the first case the energy difference in the final state (CD_4^+) after vertical transition and in its equilibrium is much smaller—about 1 eV for the lowest Jahn-Teller component in CD_4^+, as compared to about 8 eV in CD_4^{2+} (Table II). The dissociation dynamics following valence ionization should therefore be much more sensitive to the details of the potential-energy surface and our guideline calculations do not represent these features accurately. Several studies have been carried out on this topic and as a general conclusion, only some of the Jahn-Teller components can dissociate producing the CD_3^+ fragments, while others remain stable as the CD_4^+ ions [3,4,6–8]. In addition to the different dissociation products following core or valence ionization, also the line shapes in the EREICO spectra (Fig. 2) are very different. The much narrower peaks in the spectrum following the $1t_2$ ionization are explained by the smaller kinetic energy of the fragments.

Inner-valence ionization of the $2a_1$ orbital produces the CD_2^+ and CD^+ and the lack of the parent ions CD_4^+ in the ion mass spectra indicates that they are always unstable. To our knowledge, there are no theoretical studies concentrating

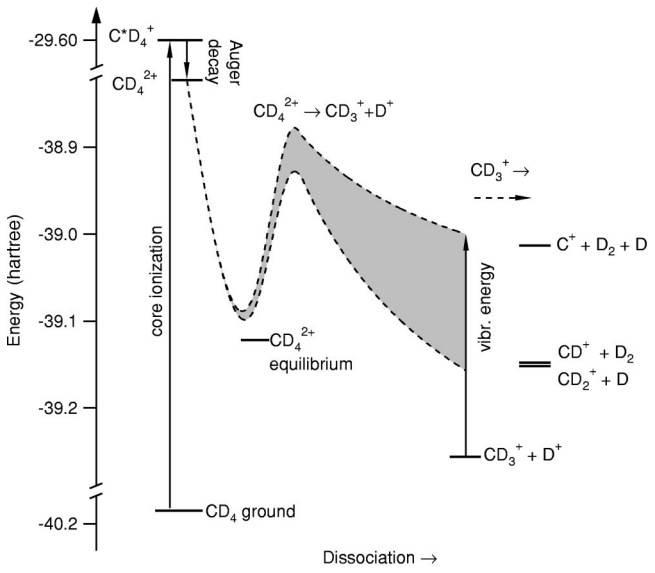

FIG. 5. A schematic diagram of the energy levels of the neutral, core-ionized, and doubly ionized CD_4 molecule and of its dissociation products. The energy levels correspond to our *ab initio* calculations and include zero-point vibrational energy. Probable dissociation routes for the first step ($CD_4^{2+} \rightarrow CD_3^+ + D^+$) are represented by the shaded area.

on the dissociation of the $2a_1^{-1}$ state. Some qualitative differences with the $1t_2^{-1}$ state are obvious: (i) There is no Jahn-Teller symmetry lowering of the $2a_1^{-1}$ state. (ii) The strongly bonding orbital $2a_1$ has the full tetrahedral symmetry of the molecule and encompasses evenly the four D atoms, whereas each of the triply degenerate $1t_2$ orbitals forms a more selective bond. This can account for the observed more general breakdown of the molecule. A comparison between the fragmentation patterns of the $2a_1^{-1}$ electronic states and the higher-lying Auger final states $2a_1^{-2}$ (see Fig. 1) would be of interest in future studies.

V. CONCLUSIONS

We have observed very different molecular fragmentation patterns following selective photoionization of the outer valence $1t_2$, inner valence $2a_1$, and the C $1s$ ($1a_1$) core orbital of the CD_4 molecule. The latter is followed by electronic Auger decay creating doubly ionized molecules. The Auger transitions to the $1t_2^{-2}$ final states cause a much more complete fragmentation of the molecule than the direct $1t_2$ valence photoionization, as demonstrated by the energy resolved electron-ion coincidence measurements, also supported by noncoincidence ion mass spectra.

Theoretical calculations of the molecular geometries and total energies were carried out for the dissociating doubly ionized molecule and for its fragments. The dynamics of the dissociation following the Auger decay was modeled by a ''dynamic walk'' procedure. Based on these results and our experimental findings, a two-step dissociation model as shown schematically in Fig. 5 is proposed. According to the dynamic walk modeling, the doubly ionized molecule first follows the reaction $CD_4^{2+} \rightarrow CD_3^+ + D^+$, in which a large ($>10$ eV) amount of potential energy is converted into the translational and vibrational energies of the fragments. In most cases, the vibrational energy of the CD_3^+ fragment is sufficient to cause a secondary dissociation producing the CD_2^+, CD^+, and even C^+ fragments, as observed in the experiment. The translational kinetic energy of these fragments is progressively smaller, as more and more of the available energy needs to be converted into vibrational energy of the CD_3^+ ion during the first stage of the dissociation (see Fig. 5). This decrease of kinetic energy towards the lighter fragments as well as the fragmentation pattern itself is indeed in good agreement with our experimental results. The sequential dissociation scenario presented in this work is an alternative to a simultaneous multiparticle dissociation. The present experiment does not yet reveal full details for the complex dissociation dynamics following core-hole decay, such as the time delay between the primary and secondary events that is predicted by the two-step model.

The vibrational motion of the core-ionized molecule, although not represented by the calculations, probably plays an important role in selecting the secondary dissociation route. Much more extensive simulations would be needed to confirm this aspect. Experimentwise, triple coincidence measurements between the Auger electrons ejected carbon $1s$ photoelectrons and ions would allow us to study the dissociation of different vibrational levels of the core-ionized state.

ACKNOWLEDGMENTS

Financial support from the Swedish Research Council (VR), Research Council of Natural Sciences and Engineering of the Academy of Finland, Polish Academy of Science, Göran Gustafsson Foundation, Wallenberg Foundation, Ragnar and Astrid Signeuls Fond, and the Lindstedts Fond is gratefully acknowledged. Help and technical support provided by the staffs of MAX-lab and BESSY-II during the experiments are appreciated. The authors also wish to thank Professor T. D. Thomas for reading and commenting on the manuscript.

[1] W. Eberhardt, E.W. Plummer, I.-W. Ly, R. Murphy, R. Carr, and W.K. Ford, Phys. Rev. Lett. **58**, 207 (1987).

[2] J.C. Creasey, H.M. Jones, D.M. Smith, R.P. Tuckett, P.A. Hatherly, K. Codling, and I. Powis, Chem. Phys. **174**, 441 (1993).

[3] T. Watanabe and S. Nishikawa, Chem. Phys. **11**, 49 (1975).

[4] E.W. van Dishoeck, W.J. van der Hart, and M. van Hemert, Chem. Phys. **50**, 45 (1980).

[5] P.A. Hatherly, M. Stankiewicz, L.J. Frasinski, K. Codling, and M.A. MacDonald, Chem. Phys. Lett. **159**, 355 (1989).

[6] J.A.R. Samson, G.N. Haddad, T. Masuoka, P.N. Pareek, and D.A.L. Kilcoyne, J. Chem. Phys. **90**, 6925 (1989).

[7] K.-M. Weitzel, M. Malow, G.K. Jarvis, T. Baer, Y. Song, and C.Y. Ng, J. Chem. Phys. **111**, 8267 (1999).
[8] C.J. Latimer, R.A. Mackie, A.M. Sands, N. Kouchi, and K.F. Dunn, J. Phys. B **32**, 2667 (1999).
[9] C.I. Ma, D.M. Hanson, K. Lee, and R.G. Hayes, J. Electron Spectrosc. Relat. Phenom. **75**, 83 (1995).
[10] G. Dujardin, D. Winkoun, and S. Leach, Phys. Rev. A **31**, 3027 (1985).
[11] E. Fainelli, F. Maracci, and L. Avaldi, J. Electron Spectrosc. Relat. Phenom. **123**, 277 (2002).
[12] Z.W. Gortel and D. Menzel, Phys. Rev. A **58**, 3699 (1998); Z.W. Gortel, R. Teshima, and D. Menzel, *ibid.* **58**, 1225 (1998).
[13] K. Ueda, M. Simon, C. Miron, N. Leclercq, R. Guillemin, P. Morin, and S. Tanaka, Phys. Rev. Lett. **83**, 3800 (1999).
[14] P. Morin, M. Simon, C. Miron, N. Leclercq, E. Kukk, J.D. Bozek, and N. Berrah, Phys. Rev. A **61**, 050701 (2000).
[15] P.A. Hatherly, J. Rius i Riu, M. Stankiewicz, F.M. Quinn, and L.J. Frasinski, J. Phys. B **35**, L77 (2002).
[16] A. Hiraya, K. Nobusada, M. Simon, K. Okada, T. Tokushima, Y. Senba, H. Yoshida, K. Kamimori, H. Okumura, Y. Shimizu, A.-L. Thomas, P. Millie, I. Koyano, and K. Ueda, Phys. Rev. A **63**, 42705 (2001).
[17] M. Bässler, A. Ausmees, M. Jurvansuu, R. Feifel, J.-O. Forsell, P. de Tarso Fonseca, A. Kivimäki, S. Sundin, S.L. Sorensen, R. Nyholm, O. Björneholm, S. Aksela, and S. Svensson, Nucl. Instrum. Methods Phys. Res. A **469**, 382 (2001).
[18] M. Stankiewicz, J. Rius i Riu, J. Álvarez, P. Erman, P. Hatherly, A. Karawajczyk, E. Kukk, M. Huttula, E. Rachlew, and P. Winiarczyk, Surf. Rev. Lett. (to be published).
[19] M. Huttula, M. Harkoma, E. Nõmmiste, and S. Aksela, Nucl. Instrum. Methods Phys. Res. A **467-468**, 1514 (2001).
[20] R.K. Nebert, J. Chem. Phys. **32**, 1114 (1960).
[21] J.C. Slater, *Quantum Theory of Molecules and Solids* (McGraw-Hill, New York, 1963), Vol. 1.
[22] C.R. Brundle, M.B. Robin, and H. Basch, J. Chem. Phys. **53**, 2196 (1970).
[23] G. Bieri and L. Åsbrink, J. Electron Spectrosc. Relat. Phenom. **20**, 149 (1980).
[24] M.C. Göthe, B. Wannberg, L. Karlsson, S. Svensson, P. Balzer, F.T. Chau, and M.-Y. Adam, J. Chem. Phys. **94**, 2536 (1991).
[25] I.B. Ortenburger and P.S. Sagus, Phys. Rev. A **11**, 1501 (1975).
[26] Z.W. Gortel, R. Teshima, and D. Menzel, Phys. Rev. A **60**, 2159 (1999).
[27] E. Kukk, J.D. Bozek, W.-T. Cheng, R.F. Fink, A.A. Wills, and N. Berrah, J. Chem. Phys. **111**, 9642 (1999).
[28] E. Kukk, A. Wills, N. Berrah, B. Langer, J.D. Bozek, O. Nayadin, M. Alserhi, A. Farhat, and D. Cubaynes, Phys. Rev. A **57**, R1485 (1998).
[29] T. Karlsen and K.J. Børve, J. Chem. Phys. **112**, 7986 (2000).
[30] T.X. Carroll, N. Berrah, J. Bozek, J. Hahne, E. Kukk, L.J. Saethre, and T.D. Thomas, Phys. Rev. A **59**, 3386 (1999).
[31] D.L. Gray and A.G. Robiette, Mol. Phys. **37**, 1901 (1979).
[32] T.H. Dunning, Jr., J. Chem. Phys. **90**, 1007 (1989).
[33] DALTON, a molecular electronic structure program, release 1.2 (2001); T. Helgaker, H.J.Aa. Jensen, P. Jørgensen, J. Olsen, K. Ruud, H. Ågren, A.A. Auer, K.L. Bak, V. Bakken, O. Christiansen, S. Coriani, P. Dahle, E.K. Dalskov, T. Enevoldsen, B. Fernandez, C. Hättig, K. Hald, A. Halkier, H. Heiberg, H. Hettema, D. Jonsson, S. Kirpekar, R. Kobayashi, H. Koch, K.V. Mikkelsen, P. Norman, M.J. Packer, T.B. Pedersen, T.A. Ruden, A. Sanchez, T. Saue, S.P.A. Sauer, B. Schimmelpfennig, K.O. Sylvester-Hvid, P.R. Taylor, and O. Vahtras, computer code DALTON, http://www.Kjemi.uio.no/software/dalton/dalton.html
[34] T. Karlsen and K.J. Børve, J. Chem. Phys. **112**, 7979 (2000).
[35] J.W. Rabalais, T. Bergmark, L.O. Werme, L. Karlsson, and K. Siegbahn, Phys. Scr. **3**, 13 (1971).
[36] H. H. Jahn and E. Teller, Proc. R. Soc. London, Ser. A **161**, 220 (1937).
[37] K. Takeshita, J. Chem. Phys. **86**, 329 (1987).
[38] O.M. Kvalheim, Chem. Phys. Lett. **86**, 159 (1982).
[39] A.F. Saturno, Theor. Chim. Acta **7**, 273 (1967).
[40] M.S. Gordon and J.M. Caldwell, J. Chem. Phys. **79**, 5503 (1979).
[41] C.F. Bender and H.F. Schaefer, III, J. Mol. Spectrosc. **37**, 423 (1971).
[42] T. Helgaker, E. Uggerud, and H.J.Aa. Jensen, Chem. Phys. Lett. **173**, 145 (1990).
[43] NIST Chemistry Webbook, URL: http://webbook.nist.gov/chemistry.
[44] *Modern Techniques in Computational Chemistry: MOTECC-90*, edited by E. Clementi (ES-COM Science Publishers B.V., The Netherlands, 1990).
[45] T. Helgaker, P. Jørgensen, and J. Olsen, *Molecular Electronic-Structure Theory* (Wiley, New York, 2000).